Available online at www.sciencedirect.com

SCIENCE DIRECT®

Earth and Planetary Science Letters 224 (2004) 547–562

EPSL

www.elsevier.com/locate/epsl

Erosional and climatic effects on long-term chemical weathering rates in granitic landscapes spanning diverse climate regimes ☆

Clifford S. Riebe[a,*], James W. Kirchner[a], Robert C. Finkel[b,c]

[a] Department of Earth and Planetary Science, University of California, Berkeley, CA 94720-4767, USA
[b] Center for Accelerator Mass Spectrometry, Lawrence Livermore National Laboratory, Livermore, CA 94551, USA
[c] Department of Earth Science, University of California, Riverside, CA 92521, USA

Received 20 November 2003; received in revised form 10 April 2004; accepted 10 May 2004

Abstract

We used cosmogenic nuclide and geochemical mass balance methods to measure long-term rates of chemical weathering and total denudation in granitic landscapes in diverse climatic regimes. Our 42 study sites encompass widely varying climatic and erosional regimes, with mean annual temperatures ranging from 2 to 25 °C, average precipitation ranging from 22 to 420 cm·year^{-1}, and denudation rates ranging from 23 to 755 t·km^{-2}·year^{-1}. Long-term chemical weathering rates range from 0 to 173 t·km^{-2} year^{-1}, in several cases exceeding the highest granitic weathering rates on record from previous work. Chemical weathering rates are highest at the sites with rapid denudation rates, consistent with strong coupling between rates of chemical weathering and mineral supply from breakdown of rock. A simple empirical relationship based on temperature, precipitation and long-term denudation rates explains 89–95% of the variation in long-term weathering rates across our network of sites. Our analysis shows that, for a given precipitation and temperature, chemical weathering rates increase proportionally with fresh-material supply rates. We refer to this as ''supply-limited'' weathering, in which fresh material is chemically depleted to roughly the same degree, regardless of its rate of supply from breakdown of rock. The temperature sensitivity of chemical weathering rates is two to four times smaller than what one would expect from laboratory measurements of activation energies for feldspar weathering and previous inter-comparisons of catchment mass-balance data from the field. Our results suggest that climate change feedbacks between temperature and silicate weathering rates may be weaker than previously thought, at least in actively eroding, unglaciated terrain similar to our study sites. To the extent that chemical weathering rates are supply-limited in mountainous landscapes, factors that regulate rates of mineral supply from erosion, such as tectonic uplift, may lead to significant fluctuations in global climate over the long term.

Keywords: chemical weathering; granitic landscape; precipitation; physical erosion; temperature; climate

1. Introduction

Chemical weathering and physical erosion act together to generate soils and sculpt landscapes. They also influence one another; physical erosion may depend on the chemical breakdown (and thus weak-

☆ Supplementary data associated with this article can be found, in the online version, at doi:10.1016/j.epsl.2004.05.019.

* Corresponding author. Tel.: +1-510-643-2171; fax: +1-510-643-9980.

E-mail addresses: riebe@seismo.berkeley.edu (C.S. Riebe), kirchner@seismo.berleley.edu (J.W. Kirchner), finkel1@llnl.gov (R.C. Finkel).

0012-821X/$ - see front matter © 2004 Elsevier B.V. All rights reserved.
doi:10.1016/j.epsl.2004.05.019

ening) of rock, and chemical weathering depends on the availability of fresh mineral surfaces created by physical erosion. Quantifying how rates of physical erosion and chemical weathering interrelate over the timescales of soil formation is therefore important for quantitative study of soil development, watershed geochemistry and landscape evolution.

Quantifying long-term rates of chemical weathering and physical erosion is also important for understanding Earth's biogeochemical cycles. For example, chemical weathering of rock helps regulate the supply of nutrients and solutes to soils, streams and the ocean, and is also the long-term sink for atmospheric CO_2, thus modulating Earth's climatic evolution via the greenhouse effect. Thus, to the extent that chemical weathering rates increase with temperature, weathering feedbacks should, over millions of years, buffer Earth's climate against large temperature shifts (e.g., [1]). To the extent that rates of chemical weathering and physical erosion are coupled, Earth's long-term climatic evolution may be regulated by physical erosion rates, with periods of increased erosion being marked by global cooling, due to increased atmospheric CO_2 consumption by weathering [2].

Chemical weathering and physical erosion should be coupled, to the degree that mineral weathering rates depend on the availability of fresh mineral surfaces with high reactivity [3,4]. Because the physical breakdown of rock regulates the supply of fresh minerals to soils, the erosion rate of bedrock should be an important control on weathering rates in soils. Results from several recent field studies [5–11] suggest that this is the case.

Chemical weathering rates have traditionally been measured either by catchment input/output mass balances (e.g., [12]), or from chemical depletion and enrichment measurements in non-eroding soils of known age [13–15]. The latter approach, based on mass balance of elements in soils and parent rock, averages weathering rates over timescales of pedogenesis, making it seemingly ideal for quantitative study of soil development, watershed geochemistry, and the long-term feedback between climate and weathering. However, because non-eroding soils of known age are rare, they have yielded few measurements of long-term chemical weathering rates. The soil mass balance approach can also be applied in mountainous settings, where soils are undergoing significant physical erosion, if the long-term rate of overall denudation can be quantified [6,16–18]. Long-term denudation rates have traditionally been difficult to measure, but they have recently become much more widely quantifiable, through application of cosmogenic nuclide methods (e.g., [19–22]). Hence, it should now be possible to quantify long-term chemical weathering rates in a greatly extended range of settings, by combining traditional, soil mass balance measurements of chemical depletion and enrichment, with cosmogenic nuclide measurements of denudation rates [6,16–18].

In previous work, we used the soil mass-balance approach to measure long-term chemical weathering rates in climatically diverse, granitic study sites in the Sierra Nevada of California, the Santa Rosa Mountains of Nevada and Rio Icacos, Puerto Rico [6,17,18]. Our results helped us validate the cosmogenic nuclide/mass balance approach (through comparison with data from other, independent approaches) [17], and enabled us to document erosional, climatic, and altitudinal effects on chemical weathering [6,18]. Here, we present data from an expanded network of field sites, and use them to quantify how climatic and erosional factors affect chemical weathering rates across a greatly extended range of climates and denudation rates. Across this network of sites, average annual precipitation varies by 19-fold, mean annual temperatures vary by 23 °C and denudation rates vary by a factor of 32, roughly doubling the range of each of these variables analyzed previously by Riebe et al. [6]. Our measurements show that rates of chemical weathering and total denudation are tightly coupled, and that the degree of chemical depletion (as measured by the ratio of the chemical weathering rate to the total denudation rate) increases systematically with temperature and precipitation.

2. Methods, field sites and sampling

2.1. Chemical weathering rates from immobile element enrichment in eroding landscapes

Our methods for estimating long-term chemical weathering rates in eroding landscapes have been de-

scribed in detail elsewhere [17]. We briefly summarize our approach here and elaborate on it further in the appendix (see online version of this article). For a soil undergoing steady-state formation, erosion and weathering (such that the mass of weathered material in storage as soil on the landscape is approximately constant through time), conservation of mass implies that the rate of conversion of rock to regolith will be equal to the total denudation rate, and it can be shown [6,17] that

$$W = D - E = D\left(1 - \frac{[\mathrm{Zr}]_{\mathrm{rock}}}{[\mathrm{Zr}]_{\mathrm{soil}}}\right) \quad (1)$$

where W is the chemical weathering flux, E is the physical erosion flux and D is the total denudation flux (i.e., the sum of W and E), all in units of mass per area per time, and $[\mathrm{Zr}]_{\mathrm{rock}}$ and $[\mathrm{Zr}]_{\mathrm{soil}}$ are the concentrations of an immobile element (in this case zirconium) in rock and soil. For dimensional consistency with the weathering flux, the rates of denudation and physical erosion in Eq. (1) are expressed as mass fluxes (not as lengths per time, as they often are elsewhere in the literature).

Eq. (1) can be rearranged to yield

$$\frac{W}{D} = \left(1 - \frac{[\mathrm{Zr}]_{\mathrm{rock}}}{[\mathrm{Zr}]_{\mathrm{soil}}}\right) = \mathrm{CDF} \quad (2)$$

where CDF, the "chemical depletion fraction", is the ratio of the chemical weathering rate to the total denudation rate [6,17,18].

Conservation-of-mass equations can also be written to express chemical weathering rates of individual elements in the rock and soil:

$$W_{\mathrm{X}} = D\left([\mathrm{X}]_{\mathrm{rock}} - [\mathrm{X}]_{\mathrm{soil}}\frac{[\mathrm{Zr}]_{\mathrm{rock}}}{[\mathrm{Zr}]_{\mathrm{soil}}}\right) \quad (3)$$

where $[\mathrm{X}]_{\mathrm{rock}}$ and $[\mathrm{X}]_{\mathrm{soil}}$ are the concentrations of an element X in rock and soil, and W_{X} is its chemical weathering rate [6,16,18].

Eq. (3) can be rearranged to yield chemical depletion fractions for individual elements ($\mathrm{CDF}_{\mathrm{X}}$):

$$\frac{W_{\mathrm{X}}}{D \cdot [\mathrm{X}]_{\mathrm{rock}}} = \left(\frac{[\mathrm{X}]_{\mathrm{rock}}}{[\mathrm{X}]_{\mathrm{soil}}} \cdot \frac{[\mathrm{Zr}]_{\mathrm{soil}}}{[\mathrm{Zr}]_{\mathrm{rock}}} - 1\right) = \mathrm{CDF}_{\mathrm{X}} \quad (4)$$

CDFs from are chemical weathering rates normalized by total denudation rates. Note that, in the steady state formulae outlined above, the denudation rate equals the rate that fresh material is supplied to soils from breakdown of rock.

2.2. Quantifying denudation rates with cosmogenic nuclides

The geochemical mass balance of Eqs. (1–4) yields chemical weathering rates of soils and their component elements from measurements of immobile element enrichment, concentrations of constituent elements in rock and soil, and total denudation rates. Denudational mass flux rates (i.e., D in Eqs. (1)–(4)) can be measured, over timescales comparable to those of soil formation, using cosmogenic nuclide techniques. ^{10}Be is produced in quartz grains near the earth's surface by cosmic ray neutrons and muons [19]. Because quartz grains at depth are shielded from cosmic radiation, cosmogenic ^{10}Be concentrations in quartz grains reflect their near-surface residence times, and can be used to infer long-term average rates of landscape denudation [20,21]. Details of how cosmogenic nuclide measurements can be used to infer denudation rates (D) for Eqs. (1)–(4) are presented in previous work [17] and in the appendix (see online version of this article).

2.3. Field sites: general information

Our 42 field sites are clustered in 14 localities (Fig. 1). In addition to new data from sites in Sonora, Chiapas, Jalisco, the Georgia Piedmont and New Zealand, our analysis includes previously published long-term rates of denudation and chemical weathering from tropical Rio Icacos, Puerto Rico [17], an altitudinal transect in the Santa Rosa Mountains, NV [18] and the Sierra Nevada, CA [6]. A compilation of site descriptions is provided in the appendix (see online version of this article). Locality names, coordinates, average climate indices and bedrock lithologies are listed in Table 1. Across our study localities, mean annual temperatures range from 2 to 25 °C and average precipitation ranges from 22 to 420 cm·year^{-1}. As Fig. 1 shows, our study sites encompass almost all possible combinations of hot/cold and wet/dry climatic regimes, making it possible to distinguish temperature effects and precipitation effects from one another. Variations in climate and dominant vegetation within each site are small, compared to

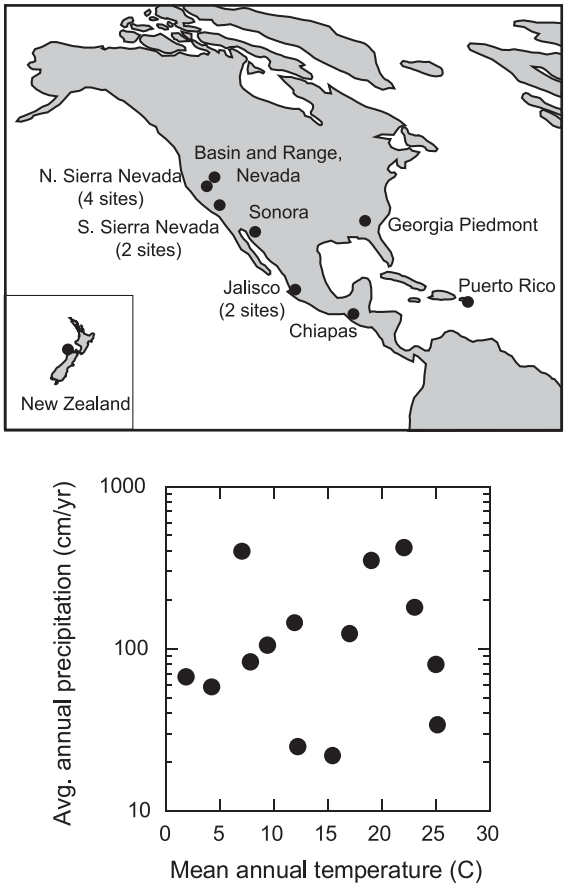

Fig. 1. Study site map (top) and plot showing precipitation and temperature characteristics (bottom). All sites are underlain by granitic bedrock and collectively span a wide range of climates, from cool, dry, high deserts to hot, humid tropical rainforests.

differences from locality to locality. Large differences in climate across the sites imply differences in erosional processes; for example, sediment transport by tree throw is probably important at forested sites, but unimportant at desert sites, which are instead prone to rainsplash erosion because they lack protective vegetative cover. All of the sites lie outside the limits of Pleistocene and Holocene glaciation, are underlain by granitic bedrock, and are situated in hilly or mountainous settings where erosion rates are significant. Soils are typically less than 60 cm thick, except at the rainforest sites where soil depths can exceed 1 m, even on the steep slopes and narrow ridgecrests typically sampled in our analysis. Soils were also typically thicker than 1 m at Panola Mountain, where topography is much more subdued than it is at our other sites. We observed no evidence of relict or buried soils (which would complicate our analysis) at any of our sites. Soils at all of our sites appear to be genetically linked to the local bedrock and typically do not exhibit strong horizonation, except in the upper 5–10 cm thick, organic-rich layer. In summary, our sites have been chosen to minimize geomorphic, lithologic and pedologic complications that could otherwise obscure the effects of erosion and climate on chemical weathering rates.

2.4. Sampling and analysis

Our sampling procedures are summarized here, and are detailed in the appendix (see online version of this article) and in previous work [6,17,18]. We collected widely distributed samples of soil and parent material (each roughly 0.5 kg) from small (0.5–10 ha) areas at each field site. Our aim was to capture any local variability in chemical weathering and avoid sampling from potentially anomalous individual points, while still sampling areas small enough that each site would represent a distinct set of climatic conditions and a roughly homogeneous lithology. We sampled soils from surfaces and also, in most cases, from depth, in order to account for potential biases due to vertical sorting by physical processes. Outcrops were sampled to represent parent material of local soils.

Denudation rates used in our weathering rate estimates (in Eqs. (1) and (3)) need to be spatially representative, to ensure consistency with element concentration measurements, which are averaged over 0.5–10 ha sampling areas. Several studies [20,21] have shown that cosmogenic nuclide concentrations in well-mixed sediment can be used to infer the average denudation rate of the sediment's source area. To apply this cosmogenic approach at our sites, we sampled sediments from hollows or channels draining each of our sites, or, at our ridgetop sites (see Table 2), from widely distributed soil surfaces. Sediment from hollows and channels should be spatially representative of eroding material in contributing areas, as should manually mixed sediment from ridgetops.

Bulk chemical and trace element compositions were measured by X-ray Fluorescence, and cosmogenic nuclide concentrations were measured by accelerator mass spectrometry. Our sample preparation and

Table 1
Characteristics of study sites

Site name	Location		Altitude range (km)	Average precipitation[a] (cm·year^{-1})	Mean annual temp.[a] (°C)	Rock type[b]	n[c]
	Latitude	Longitude					
Rio Icacos, Puerto Rico[d]	18°18′ N	67°48′ W	0.650–0.800	420	22	quartz diorite	2
McNabb Track, New Zealand	41°00′ S	172°08′ E	0.700–0.780	400	7	granite	3
Chiapas Highlands, Mexico	15°25′ N	92°30′ W	1.820–1.880	350	19	granodiorite	1
Jalisco Highlands, Mexico	20°21′ N	105°18′ W	0.750–0.820	180	23	granodiorite	4
Panola Mtn., GA, USA	33°38′ N	84°10′ W	0.220–0.280	124	17	granodiorite	1
Jalisco Lowlands, Mexico	20°08′ N	105°18′ W	0.200–0.220	80	25	granodiorite	2
Santa Rosa Mtns., NV, USA[e]	41°30′ N	117°38′ W	2.090–2.750	67	2	granodiorite	6
Sonora Desert, Mexico	29°22′ N	111°10′ W	0.320–0.510	34	25	granite	2
Northern Sierra NV, USA[f]							
Fall River	39°39′ N	121°19′ W	0.600–1.060	145	12	tonalite	4
Antelope Lake	40°10′ N	120°38′ W	1.690–1.800	83	8	grano./tonalite[b]	4
Adams Peak	39°53′ N	120°08′ W	1.890–2.250	58	4	grano./tonalite[b]	5
Fort Sage	40°10′ N	120°04′ W	1.450–1.530	25	12	grano./tonalite[b]	4
Southern Sierra NV, USA[f]							
Sunday Peak	35°47′ N	118°35′ W	2.270–2.425	105	9	granite	3
Nichols Peak	35°35′ N	118°14′ W	1.110–1.130	22	15	granodiorite	1

[a] Average precipitation and mean annual temperature reported here are averages across all study sites in each locality. Climatic variability due to orographic effects within each locality is reported in Table 2.
[b] Rock type "grano./tonalite" is intermediate between granodiorite and tonalite.
[c] n = number of catchments and/or ridgetop locations where chemical weathering rates were quantified.
[d] Rio Icacos catchments of Riebe et al. [17].
[e] Santa Rosa Mountains sites of Riebe et al. [18].
[f] Sierra Nevada sites of Riebe et al. [6,22,23].

analysis procedures are described elsewhere [6,17,18] and in the appendix (see online version of this article).

3. Results and discussion

Average temperature and precipitation estimates are presented in Table 2, along with cosmogenic nuclide concentrations, denudation rates, and chemical depletion fractions and chemical weathering rates of Na, Ca, Si and the soil as a whole.

3.1. Coupling of chemical weathering and total denudation

At Fort Sage and Fall River, denudation rates vary by a factor of 15 in response to topographic forcing from faulting and river downcutting (Table 2) [22,23], whereas CDFs (from Eq. (2)) are nearly uniform (Fig. 2A) [6]. This indicates that these sites have a nearly uniform ratio of chemical weathering rate to total denudation rate, implying that chemical weathering rates increase proportionally with total denudation rates (Fig. 2B). We term this phenomenon "supply-limited" weathering; because weathering rates are roughly proportional to the supply rate of fresh material from breakdown of rock (which equals the denudation rate under the steady-state assumptions of our analysis), soils are chemically depleted to roughly the same degree, regardless of their denudation rate.

In our analysis, chemical weathering rates are calculated, in part, from cosmogenic measurements of denudation rates, but this is not responsible for the nearly proportional relationship between weathering and denudation rates at Fort Sage and Fall River (Fig. 2B). If chemical weathering rates were not proportional to denudation rates, then the degree of Zr enrichment in soils (and thus their CDFs) would have varied systematically with denudation rates. For example, the hypothetical dashed line shown in Fig. 2B illustrates what we would have observed if chemical weathering rates were uniform across our sites. Our measurements would have shown that soils were chemically fresher at sites with faster denudation rates,

Table 2
Cosmogenic nuclide concentrations, denudation rates, chemical depletion fractions and chemical weathering rates[a]

ID	Average annual precipitation ($cm \cdot yr^{-1}$)	Mean annual temp. (°C)	Average hillslope gradient[b] ($m \cdot m^{-1}$)	[^{10}Be][c] (10^5 $at \cdot g^{-1}$)	Total denudation rate ($t \cdot km^{-2} \cdot yr^{-1}$)	Chemical depletion fractions (all in $g \cdot g^{-1}$)				Chemical weathering rates (all in $t \cdot km^{-2} \cdot yr^{-1}$)				Physical erosion rate ($t \cdot km^{-2} \cdot yr^{-1}$)
						Elemental Na	Ca	Si	Total	Elemental fluxes[d] Na	Ca	Si	Total as oxides[d]	
						CDF_{Na}	CDF_{Ca}	CDF_{Si}	CDF	W_{Na}	W_{Ca}	W_{Si}	W	
Rio Icacos, Puerto Rico														
RI-1	420	22	0.48	–[e]	87 ± 15	0.96 ± 0.01	0.97 ± 0.01	0.49 ± 0.06	0.59 ± 0.05	1.18 ± 0.27	3.96 ± 0.89	13.9 ± 3.6	51 ± 10	36 ± 7
RI-4	420	22	0.57	1.76 ± 0.10	97 ± 14	0.96 ± 0.01	0.97 ± 0.01	0.50 ± 0.02	0.61 ± 0.02	1.19 ± 0.17	4.45 ± 0.64	14.1 ± 2.1	59 ± 9	38 ± 6
McNabb Track, New Zealand														
MT-3	400	8	0.53	1.24 ± 0.07	195 ± 31	0.77 ± 0.02	0.87 ± 0.02	0.38 ± 0.06	0.45 ± 0.05	1.45 ± 0.24	2.12 ± 0.35	24.4 ± 5.4	88 ± 17	107 ± 20
MT-4	400	8	0.51	1.01 ± 0.06	235 ± 45	0.78 ± 0.03	0.87 ± 0.02	0.44 ± 0.06	0.49 ± 0.05	1.76 ± 0.35	2.56 ± 0.51	33.8 ± 8.0	115 ± 25	120 ± 26
MT-5	400	8	0.70	1.75 ± 0.10	131 ± 20	0.72 ± 0.03	0.82 ± 0.02	0.38 ± 0.04	0.44 ± 0.04	0.91 ± 0.10	1.34 ± 0.15	16.3 ± 2.5	58 ± 10	73 ± 12
Chiapas Highlands, Mexico[f]														
SS	350	19	ridgetop	2.32 ± 0.13	122 ± 14	0.84 ± 0.04	0.89 ± 0.02	0.29 ± 0.03	0.28 ± 0.03	1.37 ± 0.17	3.27 ± 0.41	10.3 ± 1.7	34 ± 6	88 ± 11
Jalisco Highlands, Mexico														
ST-1	180	23	ridgetop	0.24 ± 0.02	556 ± 71	0.60 ± 0.05	0.60 ± 0.08	0.28 ± 0.07	0.30 ± 0.06	4.14 ± 0.79	3.30 ± 0.96	53.5 ± 14.7	166 ± 42	390 ± 62
ST-3	180	23	0.50	0.63 ± 0.04	212 ± 22	0.87 ± 0.03	0.89 ± 0.03	0.37 ± 0.05	0.40 ± 0.05	2.07 ± 0.26	1.78 ± 0.24	26.8 ± 4.9	84 ± 14	128 ± 17
ST-4	180	23	ridgetop	0.21 ± 0.02	622 ± 72	0.68 ± 0.06	0.74 ± 0.06	0.22 ± 0.11	0.25 ± 0.11	5.74 ± 0.89	6.13 ± 1.22	46.0 ± 24.5	158 ± 69	464 ± 86
ST-5	180	23	0.55	0.23 ± 0.01	549 ± 59	0.74 ± 0.05	0.80 ± 0.04	0.29 ± 0.08	0.31 ± 0.07	5.48 ± 0.76	6.27 ± 1.13	52.6 ± 15.2	173 ± 44	376 ± 57
Panola Mtn., GA, USA														
PM	124	17	0.10	–[g]	23 ± 3	0.83 ± 0.02	0.87 ± 0.02	0.37 ± 0.04	0.42 ± 0.04	0.23 ± 0.03	0.27 ± 0.04	2.8 ± 0.5	10 ± 2	14 ± 2
Jalisco Lowlands, Mexico														
RT-1	80	25	ridgetop	0.20 ± 0.01	462 ± 50	0.41 ± 0.04	0.31 ± 0.05	0.24 ± 0.05	0.24 ± 0.05	2.71 ± 0.39	1.75 ± 0.34	38.5 ± 8.7	112 ± 25	350 ± 44
RT-2	80	25	ridgetop	0.23 ± 0.02	399 ± 46	0.46 ± 0.04	0.34 ± 0.06	0.26 ± 0.05	0.26 ± 0.05	2.65 ± 0.39	1.66 ± 0.38	36.3 ± 7.8	104 ± 22	296 ± 39
Santa Rosa Mtns., NV, USA														
SR-1	67	1.8	ridgetop	4.47 ± 0.25	106 ± 11	0.17 ± 0.02	0.13 ± 0.03	0.06 ± 0.02	0.07 ± 0.02	0.32 ± 0.05	0.33 ± 0.08	2.1 ± 0.8	7 ± 3	99 ± 11
SR-3	75	0.6	0.52	3.57 ± 0.20	132 ± 14	0.13 ± 0.03	0.10 ± 0.04	− 0.01 ± 0.02	0.00 ± 0.02	0.28 ± 0.07	0.20 ± 0.08	− 0.3 ± 1.0	0 ± 3	132 ± 14
SR-4	66	2.0	0.48	3.26 ± 0.19	144 ± 15	0.19 ± 0.03	0.19 ± 0.03	0.09 ± 0.02	0.10 ± 0.02	0.49 ± 0.09	0.65 ± 0.13	4.3 ± 1.2	15 ± 4	129 ± 14
SR-6	58	3.0	ridgetop	4.54 ± 0.25	104 ± 11	0.32 ± 0.03	0.32 ± 0.03	0.15 ± 0.03	0.16 ± 0.03	0.59 ± 0.08	0.73 ± 0.12	4.8 ± 1.2	16 ± 4	87 ± 10
SR-7	54	3.6	ridgetop	–[h]	117 ± 12	0.30 ± 0.05	0.29 ± 0.05	0.19 ± 0.06	0.20 ± 0.06	0.61 ± 0.12	0.77 ± 0.16	7.1 ± 2.3	24 ± 7	93 ± 12
SR-10	83	−0.4	0.55	–[h]	117 ± 12	0.16 ± 0.04	0.14 ± 0.05	− 0.03 ± 0.05	− 0.02 ± 0.05	0.31 ± 0.09	0.23 ± 0.08	− 1.1 ± 1.9	− 2 ± 6	119 ± 13
Sonora Desert, Mexico														
CE-3	34	25	ridgetop	0.59 ± 0.08	194 ± 32	0.14 ± 0.05	0.08 ± 0.06	0.17 ± 0.05	0.16 ± 0.05	0.37 ± 0.16	0.28 ± 0.22	11.2 ± 3.7	31 ± 11	163 ± 28
JC-1	34	23	ridgetop	0.65 ± 0.04	191 ± 20	0.20 ± 0.07	0.14 ± 0.08	0.17 ± 0.07	0.18 ± 0.07	0.55 ± 0.19	0.45 ± 0.29	10.9 ± 4.4	34 ± 13	158 ± 21
Fall River, N. Sierra Nevada, USA[i]														
FR-2	152	11.5	0.48	0.52 ± 0.08	485 ± 92	0.59 ± 0.07	0.54 ± 0.09	0.20 ± 0.05	0.20 ± 0.05	4.16 ± 1.26	3.40 ± 1.23	32.9 ± 10.4	99 ± 30	386 ± 77
FR-5	140	13.5	0.62	0.40 ± 0.09	384 ± 54	0.33 ± 0.03	0.30 ± 0.05	0.20 ± 0.03	0.20 ± 0.03	1.82 ± 0.34	2.65 ± 0.65	24.4 ± 5.4	75 ± 16	309 ± 45

FR-6	146	11.9	0.42	2.56 ± 0.17	104 ± 25	0.45 ± 0.06	0.38 ± 0.07	0.20 ± 0.06	0.19 ± 0.06	0.88 ± 0.24	0.65 ± 0.20	7.2 ± 2.6	19 ± 7	84 ± 21
FR-8	152	10.7	0.18	5.52 ± 0.31	40 ± 4	0.21 ± 0.11	0.11 ± 0.15	0.17 ± 0.03	0.18 ± 0.03	0.12 ± 0.08	0.05 ± 0.09	2.4 ± 0.5	7 ± 1	33 ± 4
Antelope Lake, N. Sierra Nevada, USA[i]														
AL-4	82	7.9	0.43	5.33 ± 0.35	72 ± 8	0.33 ± 0.05	0.30 ± 0.05	0.20 ± 0.05	0.21 ± 0.05	0.35 ± 0.06	0.88 ± 0.18	4.1 ± 1.2	15 ± 4	57 ± 7
AL-5	79	8.2	0.34	4.19 ± 0.31	86 ± 11	0.41 ± 0.18	0.35 ± 0.20	0.21 ± 0.23	0.22 ± 0.23	0.50 ± 0.23	1.02 ± 0.62	5.5 ± 6.0	19 ± 20	67 ± 21
AL-9	85	7.6	0.60	3.12 ± 0.21	119 ± 12	0.29 ± 0.10	0.27 ± 0.10	0.22 ± 0.11	0.22 ± 0.11	0.51 ± 0.18	1.28 ± 0.52	7.3 ± 3.7	26 ± 13	92 ± 16
AL-10	85	7.6	0.40	4.01 ± 0.27	91 ± 8	0.23 ± 0.03	0.26 ± 0.07	0.13 ± 0.04	0.13 ± 0.03	0.31 ± 0.05	1.01 ± 0.38	3.3 ± 1.2	12 ± 3	79 ± 7
Adams Peak, N. Sierra Nevada, USA[i]														
AP-3	59	4.0	0.46	3.03 ± 0.19	140 ± 13	0.24 ± 0.02	0.26 ± 0.03	0.16 ± 0.02	0.17 ± 0.02	0.52 ± 0.07	1.14 ± 0.20	6.9 ± 1.1	24 ± 3	116 ± 11
AP-4	61	3.7	0.67	4.09 ± 0.19	100 ± 9	0.16 ± 0.04	0.17 ± 0.05	0.04 ± 0.04	0.06 ± 0.04	0.24 ± 0.06	0.44 ± 0.13	1.2 ± 1.2	6 ± 4	94 ± 9
AP-5	56	4.5	0.34	2.54 ± 0.12	162 ± 15	0.22 ± 0.05	0.21 ± 0.06	0.11 ± 0.06	0.12 ± 0.06	0.56 ± 0.14	0.95 ± 0.28	5.4 ± 2.9	20 ± 9	142 ± 16
AP-11	63	3.3	0.10	5.91 ± 0.41	93 ± 12	0.31 ± 0.06	0.33 ± 0.06	0.14 ± 0.06	0.15 ± 0.06	0.44 ± 0.10	0.78 ± 0.18	4.0 ± 1.8	14 ± 6	79 ± 11
AP-13	51	5.5	0.21	3.24 ± 0.21	124 ± 12	0.28 ± 0.04	0.30 ± 0.04	0.13 ± 0.04	0.14 ± 0.04	0.55 ± 0.10	1.08 ± 0.17	5.0 ± 1.7	18 ± 6	106 ± 11
Fort Sage, N. Sierra Nevada, USA[i]														
A1	28	12.0	0.25	3.44 ± 0.26	83 ± 7	0.16 ± 0.04	0.28 ± 0.04	0.00 ± 0.05	0.06 ± 0.05	0.18 ± 0.06	0.69 ± 0.19	0.0 ± 1.3	5 ± 4	78 ± 8
A2(s)	28	12.1	0.34	–[j]	63 ± 17	0.27 ± 0.04	0.34 ± 0.05	0.18 ± 0.04	0.20 ± 0.04	0.24 ± 0.07	0.64 ± 0.20	3.5 ± 1.2	13 ± 4	50 ± 14
A3(s)	25	12.3	0.45	–[j]	173 ± 43	0.20 ± 0.06	0.21 ± 0.06	0.18 ± 0.05	0.18 ± 0.05	0.47 ± 0.19	1.03 ± 0.41	9.6 ± 3.7	32 ± 12	141 ± 36
A4(s)	25	12.5	0.63	–[j]	755 ± 263	0.18 ± 0.02	0.14 ± 0.04	0.16 ± 0.02	0.15 ± 0.02	1.93 ± 0.72	3.13 ± 1.45	37.8 ± 14.3	111 ± 43	645 ± 225
Sunday Peak, S. Sierra Nevada, USA[i]														
SP-1	103	9.8	0.55	3.19 ± 0.24	129 ± 12	0.45 ± 0.03	0.44 ± 0.05	0.14 ± 0.04	0.15 ± 0.04	0.97 ± 0.12	0.70 ± 0.12	6.1 ± 1.8	19 ± 5	110 ± 11
SP-3	105	9.5	0.45	5.06 ± 0.27	93 ± 11	0.44 ± 0.05	0.27 ± 0.07	0.04 ± 0.08	0.03 ± 0.08	0.66 ± 0.11	0.31 ± 0.09	1.2 ± 2.5	3 ± 7	90 ± 13
SP-8	108	8.9	0.21	6.06 ± 0.37	86 ± 12	0.52 ± 0.04	0.39 ± 0.07	0.11 ± 0.05	0.12 ± 0.05	0.73 ± 0.13	0.40 ± 0.09	3.1 ± 1.6	11 ± 5	75 ± 11
Nichols Peak, S. Sierra Nevada, USA[i]														
NP-1	22	15.4	0.44	1.65 ± 0.19	127 ± 12	0.16 ± 0.06	0.22 ± 0.06	0.11 ± 0.06	0.12 ± 0.06	0.29 ± 0.11	0.77 ± 0.23	4.5 ± 2.4	16 ± 7	111 ± 13

[a] Uncertainties are standard errors. Systematic uncertainty in cosmogenic nuclide production rates (equal to about 20%; Lal [19]) is not included; what matters in our analysis here are site-to-site differences in rates of denudation and chemical weathering (not their absolute values). Average element concentrations (used for CDF and W estimates) and methods for estimating denudation rates from ^{10}Be are presented in the online appendix. Physical erosion rates calculated as $D{\cdot}[Zr_{rock}]/[Zr_{soil}]$ (see Eq. (1)).

[b] Ridgetop gradients are difficult to define precisely because surfaces are curved, but we estimate them to be 0.00 m·m^{-1}, within uncertainties (± 0.03 m·m^{-1}).

[c] ^{10}Be calculated from ^{10}Be/^{9}Be measured by AMS at LLNL, and standardized against ICN ^{10}Be prepared by K. Nishiizumi (personal communication).

[d] W_{Na}, W_{Ca} and W_{Si} are elemental fluxes. Total weathering rates (from Eq. (1)) are oxide fluxes, including all elements (i.e., K, Mg, etc., in addition to Na, Ca and Si).

[e] The denudation rate of RI-1 is the inverse-variance-weighted average of RIS1 (79 ± 12 t km^{-2} year^{-1}) and RIS2 (101 ± 15 t km^{-2} year^{-1}), two amalgamated samples of soils from within the catchment. ^{10}Be concentrations of RIS1 and RIS2 are 2.06 ± 0.12 and 1.60 ± 0.09 10^5 at g^{-1} [17].

[f] The chemical depletion fractions and weathering rates of the Chiapas site are minimums (see online appendix for further details).

[g] The denudation rate of PM is taken to be the inverse-variance-weighted average of estimates inferred from two samples of alluvial sediment and one sample of surface soil from the Panola Mountain catchment. ^{10}Be concentrations in these three samples were 4.39 ± 0.24, 4.80 ± 0.28 and 6.45 ± 0.36 10^5 at g^{-1}, corresponding to denudation rates of 29 ± 7, 30 ± 7 and 19 ± 4 t km^{-2} year^{-1}, respectively.

[h] No cosmogenic nuclide data are available for SR-7 and SR-10. Denudation rates are assumed to be the average of other four sites at the Santa Rosa Mountains locality. This should be reasonable given that denudation rates vary by only a factor of 1.4 across the sites. Moreover, the chemical depletion fraction of SR-10 is 0 within uncertainties, implying that the chemical weathering rate there must also be 0 (see Eq. (1)), independent of denudation rate [18].

[i] Sierra Nevada sites of Riebe et al. [6]. Denudation rates are revised according to calculation procedures of Riebe et al. [17] and are averages of estimates inferred from cosmogenic ^{10}Be and ^{26}Al concentrations. ^{26}Al concentrations are reported in Riebe et al. [22]. Weathering rates of FR-2, FR-5, AL-4, A2, SP-1 and NP-1 are revised slightly (see online appendix for details). NP-18 is excluded because only one sample of its soil's parent material is available. None of these modifications significantly affect the analysis and conclusions presented here. Temperature values scaled from locality-wide averages reported in Riebe et al. [22] using lapse rate = – 6 °C/km.

[j] See Granger et al. [21] for ^{10}Be data from Fort Sage. Denudation rates inferred using subtraction of areas method (after [21]).

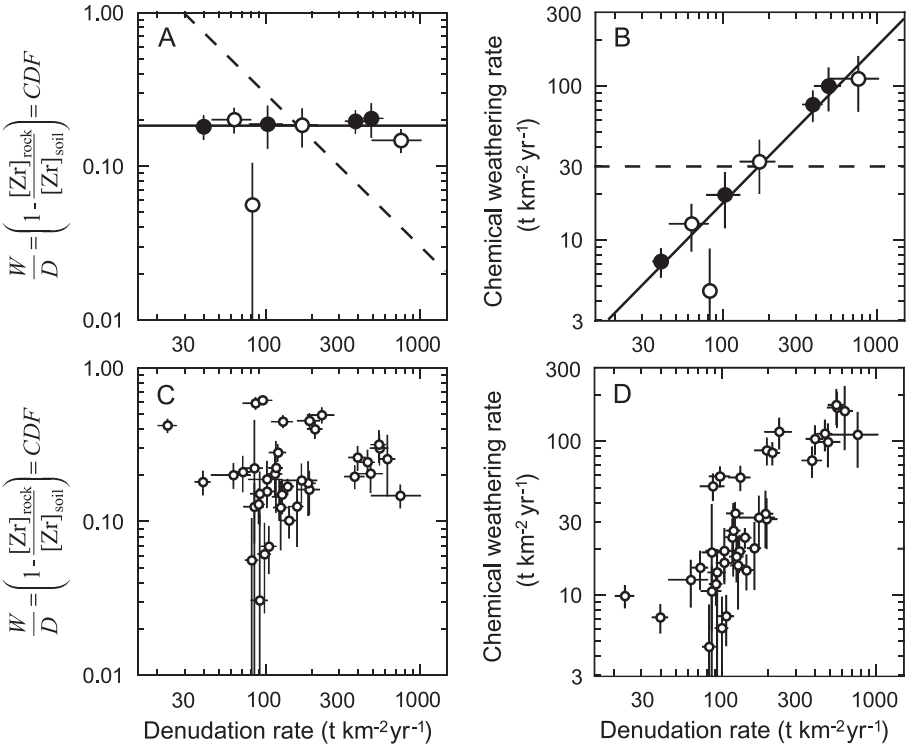

Fig. 2. Chemical depletion fractions (the ratio of chemical weathering rates to total denudation rates) (A, C) and chemical weathering rates (B, D) plotted against denudation rates for sites at Fort Sage (open circles) and Fall River (closed circles), 2 Sierra Nevada localities where denudation rates vary substantially (A, B), and for all 42 field sites (C, D). CDFs are roughly uniform across Fall River and Fort Sage (A), implying that chemical weathering rates increase proportionally with denudation rates (B). Hypothetical dashed lines shown in A and B illustrate what we would have observed if chemical weathering rates were more uniform across our sites (dashed line in B), and thus if soils were chemically fresher at sites with faster denudation rates, leading to a decrease in CDFs with increasing denudation rates (dashed line in A). Across all of the sites, CDFs are not strongly correlated with denudation rates (C), indicating that the degree of chemical depletion of soils is not sensitive to the rate of supply of minerals by incorporation of rock into soil. This implies that chemical weathering rates are higher in areas of more rapid denudation (D); to achieve the same degree of chemical depletion when denudation rates are faster, chemical weathering rates must also be faster.

and thus CDFs would have decreased with increasing denudation rates (dashed line in Fig. 2A). Indeed, this would have been consistent with our original working hypothesis; because temperature and precipitation do not vary significantly at either Fort Sage or Fall River, we expected that weathering rates would be roughly uniform there, and CDFs would be inversely proportional to denudation rates. Instead, the degree of chemical alteration (as measured by the enrichment of Zr and expressed by the CDF) is nearly constant across a wide range of denudation rates, implying that rates of chemical weathering must be roughly proportional to rates of denudation.

The trends observed at Fall River and Fort Sage also generally hold across all of our 42 sites; denudation rates vary widely (by a factor of 32), but have a negligible effect on chemical depletion fractions (Fig. 2C), and thus have a roughly proportional overall effect on chemical weathering rates (Fig. 2D). Two different mechanisms could help generate the strong coupling between rates of chemical weathering and total denudation shown in Fig. 2D. First, chemical weathering may be strongly regulated by rates that mineral surfaces are made available for chemical attack by physical breakdown of rock. Second (and conversely), rates of rock breakdown may depend on weakening caused by chemical weathering. We suspect that the first mechanism may be dominant at our sites; in previous analyses, we have shown that rapid denudation (and thus rock breakdown) tends to occur in areas of rapid base-

level lowering [22,23], implying that denudation rates can be strongly regulated by tectonic forcing.

Denudation rates can vary by more than an order of magnitude in a single climatic regime (Fig. 2A,B) and are strongly coupled to rates of chemical weathering (Fig. 2D). This implies that site-to-site differences in denudation rates can often obscure the effects of climatic variables on chemical weathering rates. This is readily apparent across our 42 sites. For example, differences in denudation rates, not climatic factors, help explain why Si weathering rates at 11 of the sites exceed the 12–23 $t_{Si}\cdot km^{-2}\cdot year^{-1}$ range reported for Rio Icacos [17], which were the highest weathering rates previously measured for granite [4,12]. Our Jalisco Highlands, Mexico sites ST-1 and ST-5 both have Si weathering rates of 53 $t_{Si}\cdot km^{-2}\cdot year^{-1}$ (Table 2), over twice the rate reported for Rio Icacos. The other Jalisco Highlands sites also surpass Rio Icacos in both Si and total weathering rates, as do our two Jalisco Lowlands sites, two of our McNabb Track, New Zealand sites and three sites at Fall River and Fort Sage, in the northern Sierra Nevada. In all 11 cases, denudation rates are significantly higher (by up to a factor of 8) than they are at Rio Icacos (Table 2). Hence, even though weathering intensities should be relatively low at those sites (because they are all drier and/or cooler than Rio Icacos), chemical weathering rates are still relatively high, because rates of mineral supply from conversion of rock to regolith are also relatively high.

Fig. 3 shows further evidence that differences in denudation rates confound climatic effects on chemical weathering. Chemical weathering rates vary by almost as much at any given precipitation (Fig. 3A) and temperature (Fig. 3B) as they do across the spectrum of climatic conditions encompassed by the sites. This is at least partly because denudation rates vary significantly within some of the individual climatic regimes (Fig. 2B,D). By contrast, CDFs (i.e., chemical weathering rates normalized by total denudation rates) are either uniform (Fig. 2A) or can be grouped into relatively tight distributions within each climatic regime (Table 2). Moreover, these CDF groupings can be readily interpreted in terms of climate differences across the sites. For example, wet sites including both cool and hot examples (i.e., McNabb Track and Rio Icacos) have the highest CDFs (>0.5). By comparison, the Jalisco Highlands sites have lower CDFs, of roughly 0.25–0.4, consistent with their markedly lower average precipitation and slightly higher mean annual temperature. The more temperate sites (in the Sierra Nevada and Santa Rosa Mountains) have even lower CDFs, with most less than 0.2 [6,18], and some, at the coldest sites, dipping as low as zero within error [18]. These relationships are illustrated graphically in Fig. 3; CDFs increase systematically with average annual precipitation (Fig. 3C) and also with mean annual temperature (Fig. 3D), when competing precipitation effects are taken into account (see outliers and Fig. 3 caption).

Taken together, these results indicate that quantifying climatic effects on chemical weathering rates requires (a) accounting for site-to-site differences in denudation rates and (b) separating the effects of temperature and precipitation. Below, we outline a simple empirical model that takes these considerations into account.

3.2. Quantifying erosional and climatic effects on chemical weathering

Silicate mineral weathering kinetics have been conventionally modeled with the Arrhenius equation [12,24]:

$$W_X = A \cdot \exp\left[-\frac{Ea_X}{RT}\right] \quad (5)$$

where A is an empirical constant that subsumes the effects of surface area and reactivity, Ea_X is the activation energy for the weathering reaction that releases element X, R is the universal gas constant and T is absolute temperature in Kelvin. Although the Arrhenius equation is strictly applicable to weathering reactions of individual minerals, it has also been applied to elemental weathering rates [4,12], under the tacit assumption that the weathering flux of an individual element will be dominated by dissolution of a single mineral, and thus will be characterized by a single activation energy.

In their empirical analysis of climatic effects on short-term average weathering rates from granitic terrain, White and Blum [12] adapted Eq. (5) to include a linear function of precipitation. We adopt a similar formulation, but instead use a power function to retain flexibility for the fit. Runoff would be somewhat more appropriate than precipitation (be-

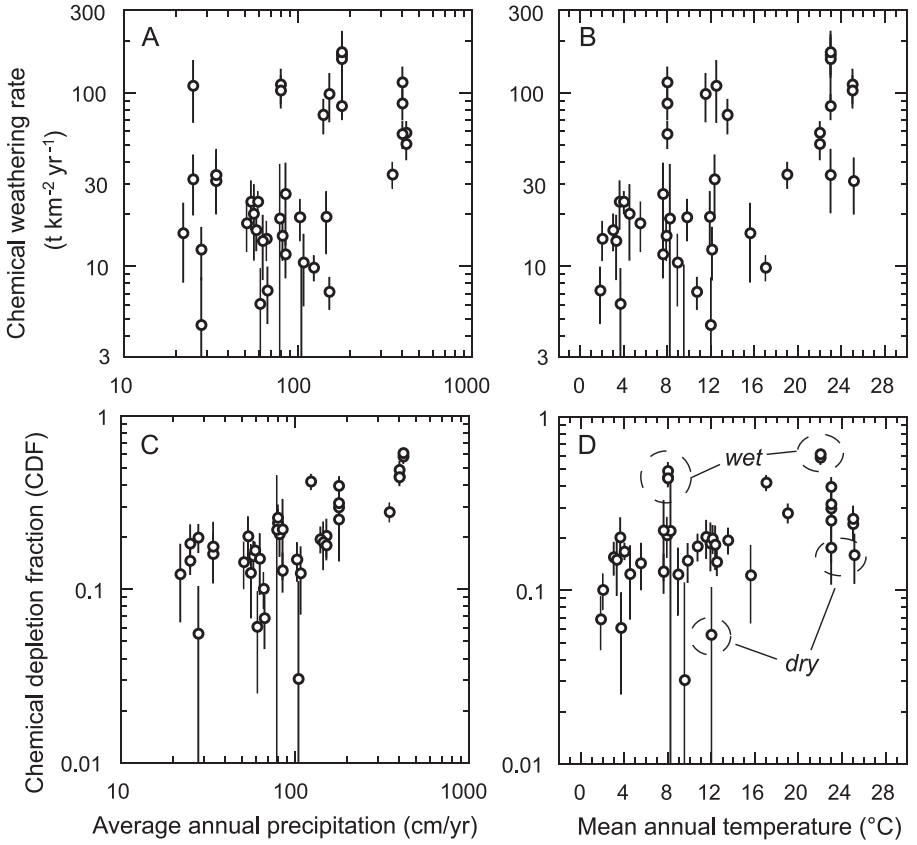

Fig. 3. Chemical weathering rates (A, B) and chemical depletion fractions (C, D) plotted against average annual precipitation (A, C) and mean annual temperature (B, D). As much as an order of magnitude or more of variation in chemical weathering rates within each site (A and B) make any relationships between chemical weathering rates and climate across the sites difficult to identify. Our analysis suggests that this is at least partly due to variations in the rates that fresh minerals are supplied by incorporation of rock into soil (see Fig. 2 and text). Conversely, CDFs increase with both average precipitation (C) and temperature (D) when effects of precipitation are taken into account; effects of precipitation appear to dominate as the climatic factor determining weathering rates, with data from our wettest, coolest sites (e.g., McNabb Track) plotting relatively high, and data from our hottest, driest sites (e.g., Sonora Desert) plotting relatively low, compared to the CDF-temperature trend exhibited by the rest of the data (see outliers circled and labeled in D).

cause it more directly reflects the volume of water reacting with soils) but is not generally available at the small hillslope scales considered here. To account for site-to-site differences in mineral supply rates, we incorporate a power function of the denudation rate ($D{\cdot}[\mathrm{X}]_{\mathrm{rock}}$, equal to the rate of fresh-material supply in steady state) into our model for W_{X}:

$$W_{\mathrm{X}} = a_{\mathrm{X}} \cdot \mathrm{AAP}^{b_{\mathrm{X}}} \cdot \exp\left(-\frac{\mathrm{Ea}_{\mathrm{X}}}{RT}\right) \cdot \left(D \cdot [\mathrm{X}]_{\mathrm{rock}}\right)^{c_{\mathrm{X}}} \quad (6)$$

where AAP is average annual precipitation rate and a_{X}, b_{X}, c_{X} and Ea_{X} are fitted constants.

Eq. (6), linearized for multiple regression, becomes

$$\ln(W_{\mathrm{X}}) = \ln(a_{\mathrm{X}}) + b_{\mathrm{X}} \cdot \ln\left(\frac{\mathrm{AAP}}{\mathrm{AAP}_{\mathrm{ref}}}\right) + \frac{\mathrm{Ea}_{\mathrm{X}}}{R} \cdot \left(\frac{1}{T_{\mathrm{ref}}} - \frac{1}{T}\right) + c_{\mathrm{X}} \cdot \ln\left(\frac{D \cdot [\mathrm{X}]_{\mathrm{rock}}}{\left(D \cdot [\mathrm{X}]_{\mathrm{rock}}\right)_{\mathrm{ref}}}\right) \quad (7)$$

where $\mathrm{AAP}_{\mathrm{ref}}$ and T_{ref} are constant reference values for precipitation and temperature, taken to be the means for our 42 study sites (113 cm year^{-1} and 12 °C), and $(D{\cdot}[\mathrm{X}]_{\mathrm{rock}})_{\mathrm{ref}}$, also a constant reference value, is the mean rate of fresh-material supply (reported in Table 3

Table 3
Summary of model parameters and Sutcliffe-Nash statistics of model efficiency

Element	a_X	b_X	c_X	Average rate of fresh-material supply $D\cdot[X]_{rock}$ [a]	Apparent activation energy ($kJ\cdot mol^{-1}$)	Sutcliffe-Nash statistics [b]	
						W_X	CDF_X
Na	1.2 ± 0.1	0.57 ± 0.06	0.96 ± 0.07	2.8	17 ± 5	0.95	0.84
Ca	1.6 ± 0.1	0.59 ± 0.09	1.03 ± 0.10	3.9	14 ± 7	0.93	0.78
Si	12.9 ± 1.0	0.36 ± 0.09	0.95 ± 0.10	64.7	24 ± 7	0.89	0.67
Soil (total)	42.5 ± 3.8	0.42 ± 0.09	0.98 ± 0.11	197.7	20 ± 8	0.91	0.69

[a] Average $D\cdot[X]_{rock}$ is used as the constant reference value for fresh-material supply rates in Eqs. (7) and (8).
[b] This statistic expresses the fraction of the variance in the data that is explained by the model (equal to R^2 for the regression).

for each element). Including reference values in our regression makes a_X a meaningful constant, equal to W_X under reference conditions.

We used Eq. (7) to estimate how weathering rates of Na, Ca, Si and the soil as a whole depend on temperature, precipitation and mineral supply rates. The regression slopes, reported in Table 3, are all statistically significant at $p < 0.05$. We assess the goodness-of-fit for each regression using Sutcliffe-Nash statistics, which express the fraction of the variance in weathering rates that is explained by the model fit. Table 3 shows that, for Na, Ca, Si and the soil as a whole, 95%, 93%, 89% and 91% of the variance in chemical weathering rates can be explained by site-to-site differences in average precipitation, temperature and rates of mineral supply. The agreement between observed and predicted W_X's is shown in Fig. 4A,C,E,G. Predicted weathering rates in Fig. 4 stray significantly from the 1:1 line for only a few of the 42 sites, verifying that the simple regression model can explain weathering rates across a wide range of denudation rates and climatic conditions. However, we note that, in the limit of high precipitation and temperature, Eq. (7) will predict weathering rates that exceed measured total denudation rates (which would be impossible, because $D = W + E$). Therefore, Eq. (7) should be considered an empirical model for mineral weathering rates under the range of climates considered here, rather than a mechanistic model for weathering under all possible climatic conditions.

For the entire network of sites, c_X equals unity within uncertainties for all elements (Table 3), indicating that, for a given precipitation and temperature, there is near proportional, supply-limited coupling of rates of chemical weathering and total denudation. From a statistical standpoint, this result could hypothetically arise from artifactual correlation between measured values of D and calculated values of W, which depend in part on D itself. However, as discussed in Section 3.1 above, W is roughly proportional to D only because the degree of Zr enrichment is independent of denudation rates, implying that weathering rates must be faster at sites with higher denudation rates. Across our sites, variations in chemical weathering rates would have been less strongly coupled to variations in denudation rates (even though W_X is calculated from D), if soils were chemically fresher at more rapidly eroding sites. Our analysis would have reflected this in lower estimated values for the exponent c_X. Furthermore, as discussed in Section 3.3 below, Eq. (7) explains nearly as much of the variation in CDFs (which do not depend on measured denudation rates) as it does the variation in weathering rates. Thus, artifactual correlation can only account for a small fraction of the variance in chemical weathering rates that is explained by Eq. (7). In fact, Eq. (7) is no more circular than equations that express how solute-flux based estimates of weathering rates (e.g., [4,12]) vary with precipitation or runoff (which is used to calculate solute fluxes—and thus weathering rates—themselves).

3.3. Predicted chemical depletion fractions

As a further test of our model's performance, we use it to predict chemical depletion fractions, for comparison with what we infer from Eqs. (2) and (4):

$$CDF_X = \frac{a_X \cdot \left(\frac{AAP}{AAP_{ref}}\right)^{b_X} \cdot \exp\left(-\frac{Ea_X}{R}\cdot\left(\frac{1}{T_{ref}}-\frac{1}{T}\right)\right)\cdot\left(\frac{D\cdot[X]_{rock}}{(D\cdot[X]_{rock})_{ref}}\right)^{c_X}}{D\cdot[X]_{rock}} \quad (8)$$

For our sites, with c_X roughly equal to unity, the right side of Eq. (8) effectively reduces to the precipitation and temperature terms. Thus, Eq. (8) indicates

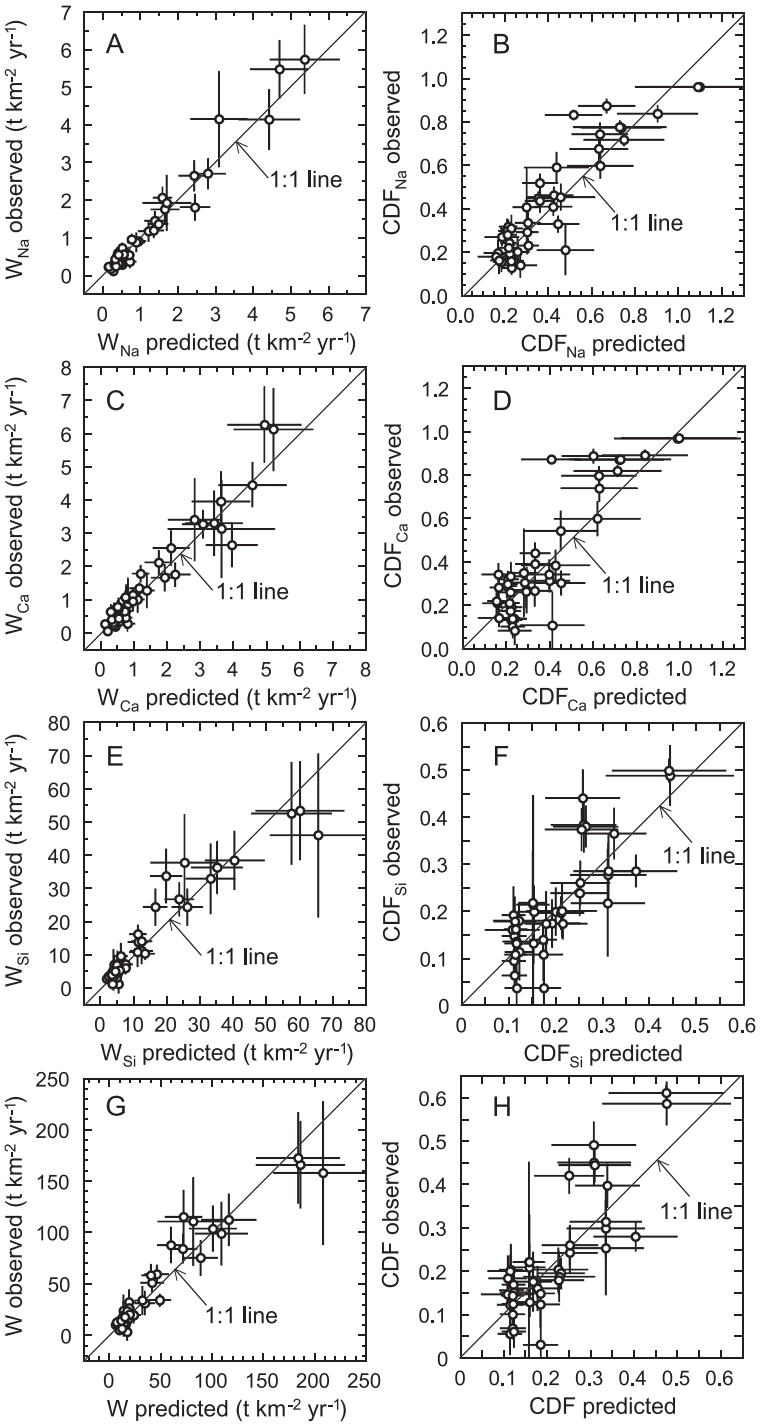

Fig. 4. Observed versus predicted chemical weathering rates (A, C, E, G) and chemical depletion fractions (B, D, F, H) for individual elements Na (A–B), Ca (C–D) and Si (E–F), and for the soil as a whole (G–H). Predicted values obtained from the models of Eq. (7) (for A, C, E, G) and Eq. (8) (for B, D, F, H), using best-fit parameter values listed in Table 3. Uncertainties are propagated from standard errors of measurements and parameter estimates.

that, for sites exhibiting "supply-limited" weathering ($c_X = 1$), climatic effects on chemical weathering should be strongly reflected in site-to-site differences in chemical depletion fractions. This is consistent both with the relatively tight groupings of CDFs according to climatic regime (discussed in Section 3.1) and with what we observe in Fig. 3C,D. Moreover, Eq. (8), coupled with our cosmogenic measurements of total denudation rates and the regression parameters estimated from Eq. (7), can explain 67–84% of the variance in observed chemical depletion fractions (see Sutcliffe-Nash statistics in Table 3), quantitatively confirming that CDFs are well explained by differences in temperature and precipitation across our sites. The correspondence between observed CDFs and values predicted from Eq. (8) is illustrated in Fig. 4B,D,F,H.

3.4. Supply-limited versus weathering-limited behavior

Linkages between chemical weathering, physical erosion and mineral supply rates have been highlighted in several recent studies of actively eroding mountainous catchments [7,8,10,11], and also larger basins, incorporating mountains and lowlands [5,9]. Results from these studies are broadly consistent with our results, but several differences merit discussion. For example, in rapidly uplifting catchments along the Alpine Fault, New Zealand, solute concentrations and Sr ratios in stream water suggest that silicate weathering rates there are elevated by a factor of roughly two, compared to areas with lower denudation rates [11]. This implies that rates of chemical weathering and total denudation are coupled, but suggests that the coupling may be less pronounced than the proportional correspondence we observe in Fig. 2B,D and obtain from Eq. (7) (c_X values ≈ 1 in Table 3). However, rates of uplift and denudation in the New Zealand catchments are much higher than any considered in our analysis, raising the possibility that there is some threshold between the strongly supply-limited weathering observed here (Fig. 2, Table 3) for moderate denudation rates, and the more weathering-limited [3] behavior for rapid denudation, implied by the New Zealand data [11]. Such a threshold would be consistent with weathering rates keeping pace with increasing denudation rates up to a point, after which rates of fresh mineral supply and removal by erosion are so fast that weathering fails to chemically deplete soils to the degree it could under lower supply rates. Weathering behavior similar to that exhibited by the rapidly eroding New Zealand catchments (i.e., with c_X less than 1) has also been suggested by studies of larger, more slowly eroding basins [5,9]. However, direct comparisons with those studies are problematic. Our estimates of long-term rates of chemical weathering and total denudation come directly from the hillslopes where the rock is eroding and weathering. By contrast, estimates based on suspended sediment and solute concentrations in large rivers [5,9] may only weakly reflect rates of primary sediment and solute production on slopes, due to effects of episodic erosion [25] and secondary storage, erosion [26] and weathering in floodplains and colluvial hollows.

3.5. Temperature-dependence of chemical weathering rates

The range of apparent activation energies shown in Table 3 is 14–24 $kJ \cdot mol^{-1}$, roughly a factor of 2–4 lower than the 45–85 $kJ \cdot mol^{-1}$ range that has been reported for feldspar weathering rates in laboratory experiments [12,24] and also for catchment mass-balance weathering fluxes of Na and Si in the field [4,8,12]. To the extent that weathering reactions are strongly influenced by biological processes (e.g., [27,28]), they may have different effective activation energies than abiotic weathering reactions in the laboratory. In the field, vegetation and soil microbes promote weathering by modifying pH, by altering physical properties in soils, and by generating chelating ligands, organic acids and CO_2 [29]. To the extent that these biological processes catalyze weathering reactions in the field, they should both accelerate them and reduce their effective activation energy, making them less temperature-sensitive. However, in climatic regimes that are extreme enough to substantially alter biological activity, the temperature-dependence of weathering rates may largely reflect the temperature sensitivity of biological processes. For example, weathering rates are much more sensitive to temperature than one would expect from typical silicate weathering activation energies among our Santa Rosa Mountains sites, which lie along an altitude transect reaching from below the treeline into the alpine zone [18]. Drever and Zobrist [30] similarly found greater-than-expected temperature

sensitivity in weathering rates inferred from stream solute concentrations across an altitude transect in the Swiss Alps. Conversely, one might expect weathering rates to increase more slowly (or even decrease) with increasing temperature, as conditions become hot and dry enough to inhibit biological activity. There is some suggestion of such a biological threshold at our two Sonora Desert sites, which plot below the trend lines for the other sites in Fig. 4.

To the extent that weathering of biotite, hornblende and other phases in our rocks is more or less temperature sensitive than feldspar weathering, we might expect whole-rock activation energies from our field-based, elemental weathering rates to be different from values reported for feldspar in the laboratory. For example, Ca has been shown to weather rapidly from calcite in the early stages of granite weathering [31]. Moreover, there is some suggestion, based on bulk weathering of granitic rocks in batch reactors [4], that differences in mineral composition (i.e., proportions of feldspars, biotite and hornblende) might lead to differences in apparent activation energies for some elements. Hence, the fact that our analysis considers weathering from several different types of granites might help explain the differences between the activation energies reported in Table 3 and those determined from laboratory experiments. However, it cannot explain the differences between our results and other field studies, which are also based on whole-rock weathering in granites of varying composition.

Our estimates of air temperature are inexact indicators of conditions for weathering in soils. Moreover, seasonal temperature effects may be important and could be masked by our use of mean annual temperature. Both of these factors could lead to differences between field- and lab-based activation energies, but are unlikely to explain large differences among the field-based studies, which are all subject to the same liabilities in climate parameterization (because they all use mean annual air temperature).

While previous field-based studies generally share many of the same limitations as ours, our estimates of temperature sensitivity cannot be compared straightforwardly with those from catchment mass-balance studies [4,8,12] for at least two reasons. First, our analysis demonstrates that physical erosion and chemical weathering are tightly coupled, and explicitly accounts for this interrelationship. Previous compilations of weathering rates have often been unable to take potentially confounding variations in erosion rates into account, because erosion rates have traditionally been difficult to measure accurately. Second, our analysis is confined to actively eroding, unglaciated terrain. By contrast, previous compilations of field weathering rates have typically combined unglaciated and recently glaciated sites (which might be expected to have transiently high weathering rates; e.g., [15]), again potentially confounding the effects of climatic variations on weathering rates. More work is needed to clarify the effects of climate on weathering rates under field conditions.

Our mass-balance approach averages chemical weathering rates over thousands of years, whereas instrumental records used to determine climate in our analysis span years to decades, raising the possibility that ambient climate may have differed significantly over the two time scales. However, these differences should have a relatively small effect on results from our study, for several reasons. First, Holocene climate changes were largely synchronous across North America [32], implying that they affected most of our sites as a whole, and would not have substantially altered the site-to-site climatic differences on which our analysis is based. Second, for mid- to low-latitude sites, glacial-to-interglacial warming has been estimated at only ~ 5 °C [33], much less than the 23 °C temperature range encompassed by our sites. Thus, while present-day climatic conditions will not precisely reflect long-term average climate, the large site-to-site climatic differences considered in our analysis have probably been largely preserved. Third, at the colder sites (in the Sierra Nevada and Santa Rosa Mountains), where 5 °C of warming would shorten the seasonal duration of freezing (and thus weathering inhibition), regional data [34] suggest more moderate (2 °C) warming over the late Holocene. Fourth, the mountain soils considered in our analysis are thin, implying short (order 7000 years [18]) residence times, with minimal exposure to climate and vegetation change. Hence, the temperature and precipitation observed today should largely reflect climatic conditions over the timescales of soil formation at our sites, implying that the effects of climate change should be fairly small. Measurements from Rio Icacos, Puerto Rico suggest that this is the case; long-term weathering rates from our mass-balance approach agree with two independent meas-

urements of short-term weathering rates [17], even though soil thickness and residence time are both greater at Rio Icacos than at most of our other sites. Taken together, these considerations suggest that our analysis should provide robust estimates of the temperature sensitivity of chemical weathering rates.

4. Conclusions and implications

Our analysis of climatic influences on chemical weathering includes long-term weathering rates from diverse granitic sites, spanning 2–25 °C in mean annual temperature and 22–420 cm $year^{-1}$ in average precipitation. Cosmogenic nuclides show that long-term denudation rates vary by more than 30-fold across our sites. Long-term chemical weathering rates, calculated from denudation rates and CDFs, span a range of 0–173 $t \cdot km^{-2} \cdot year^{-1}$ and include the most rapid chemical weathering rates on record for unglaciated granitic terrain. Chemical weathering rates are highest at sites undergoing rapid erosion, and moreover are tightly coupled with denudation rates across the entire data set, implying that chemical weathering rates are sensitive to rates that fresh material is supplied to soils from physical breakdown of rock.

Regression analyses show that up to 95% of the variance in chemical weathering rates of Na, Ca, Si and the soil as a whole can be predicted using the product of a power function of precipitation, an Arrhenius-like function of temperature, and a power function of the fresh-material supply rate (equal to the denudation rate, under the steady state assumptions of our analysis). Our analyses indicate that, for a given precipitation and temperature, weathering is ''supply-limited'': chemical weathering rates increase proportionally with rates of fresh-material supply, such that fresh material is chemically depleted to roughly the same degree, regardless of its rate of supply from breakdown of rock. Temperature and precipitation explain 67–84% of the variance in CDFs across our sites, highlighting the importance of climatic influences on chemical weathering.

Our regression analyses indicate that the temperature sensitivity of long-term chemical weathering rates is a factor of roughly 2–4 lower than the range that has been reported for short-term weathering rates from the field and the lab. If this result is more generally true for other actively eroding, granitic landscapes (such as those considered here), and also for other rock types, then it implies that feedbacks between climate change and primary silicate weathering in unglaciated mountainous settings may be only a weak buffer against long-term global temperature shifts. The strong coupling between chemical weathering and total denudation measured in our analysis implies that, by regulating denudation rates, tectonic uplift may be an important regulator of chemical weathering rates, particularly in areas where supply-limited weathering prevails. Further work is needed clarify whether plausible changes in uplift rates in such areas could alter silicate weathering (and thus CO_2 consumption) rates enough to cause significant fluctuations in global climate over the long term.

Acknowledgements

We thank C. Bechtel, M. Fantle, T. Ramírez and F. Solis for field assistance; A. White for contributing to our Panola Mountain samples; J. Troester, F. Scatena, J. Roering, M. Hansen, D. McNabb, B. Chalmers and N. Peters for logistical assistance; L. Glaser and T. Teague for lab assistance; and J. Blum and J. Gaillardet for helpful reviews. Access to Kahurangi National Park was granted by the N. Zealand Department of Conservation. Access to Luquillo Experimental Forest, Puerto Rico was granted by the U.S. Forest Service, under the U.S. Geological Survey WEBB program. This work was supported by NSF grant EAR-0000999 to Kirchner. ^{10}Be measurements were performed under the auspices of the U.S. Department of Energy by the University of California, Lawrence Livermore National Laboratory, under contract W-7405-Eng-48. ***[KF]***

References

[1] R.A. Berner, A.C. Lasaga, R.M. Garrels, The carbonate-silicate geochemical cycle and its effect on atmospheric carbon-dioxide over the past 100 million years, Am. J. Sci. 283 (1983) 641–683.

[2] M.E. Raymo, W.F. Ruddiman, P.N. Froelich, Influence of late Cenozoic mountain building on ocean geochemical cycles, Geology 16 (1988) 649–653.

[3] R.F. Stallard, J.M. Edmond, Geochemistry of the Amazon: 2.

The influence of geology and weathering environment on the dissolved load, J. Geophys. Res. 88 (1983) 9671–9688.
[4] A.F. White, A.E. Blum, T.D. Bullen, D.V. Vivit, M. Schulz, J. Fitzpatrick, The effect of temperature on experimental and natural chemical weathering rates of granitoid rocks, Geochim. Cosmochim. Acta 63 (1999) 3277–3291.
[5] J. Gaillardet, B. Dupré, P. Louvat, C.J. Allègre, Global silicate weathering and CO_2 consumption rates deduced from the chemistry of large rivers, Chem. Geol. 159 (1999) 3–30.
[6] C.S. Riebe, J.W. Kirchner, D.E. Granger, R.C. Finkel, Strong tectonic and weak climatic control of long-term chemical weathering rates, Geology 29 (2001) 511–514.
[7] S.P. Anderson, W.E. Dietrich, G.H. Brimhall, Weathering profiles, mass-balance analysis, and rates of solute loss; linkages between weathering and erosion in a small steep catchment, Geol. Soc. Amer. Bull. 114 (2002) 1143–1158.
[8] T.K. Dalai, S. Krishnaswami, M.M. Sarin, Major ion chemistry in the headwaters of the Yamuna river system: chemical weathering, its temperature dependence and CO_2 consumption in the Himalaya, Geochim. Cosmochim. Acta 66 (2002) 3397–3416.
[9] R. Millot, J. Gaillardet, B. Dupré, C.J. Allègre, The global control of silicate weathering rates and the coupling with physical erosion; new insights from rivers of the Canadian Shield, Earth Planet. Sci. Lett. 196 (2002) 83–98.
[10] A.J. West, M.J. Bickle, R. Collins, J. Brasington, Small-catchment perspective on Himalayan weathering fluxes, Geology 30 (2002) 355–358.
[11] A.D. Jacobson, J.D. Blum, Relationship between mechanical erosion and atmospheric CO_2 consumption in the New Zealand Southern Alps, Geology 31 (2003) 865–868.
[12] A.F. White, A.E. Blum, Effects of climate on chemical weathering in watersheds, Geochim. Cosmochim. Acta 59 (1995) 1729–1747.
[13] R. April, R. Newton, L.T. Coles, Chemical weathering in two Adirondack watersheds: past and present day rates, Geol. Soc. Amer. Bull. 97 (1986) 1232–1238.
[14] G.H. Brimhall, W.E. Dietrich, Constitutive mass balance relations between chemical-composition, volume, density, porosity, and strain in metasomatic hydrochemical systems—results on weathering and pedogenesis, Geochim. Cosmochim. Acta 51 (1987) 567–587.
[15] A. Taylor, J.D. Blum, Relation between soil age and silicate weathering rates determined from the chemical evolution of a glacial chronosequence, Geology 23 (1995) 979–982.
[16] J.W. Kirchner, D.E. Granger, C.S. Riebe, Cosmogenic isotope methods for measuring catchment erosion and weathering rates, J. Conf. Abstr. 2 (1997) 217.
[17] C.S. Riebe, J.W. Kirchner, R.C. Finkel, Long-term rates of chemical weathering and physical erosion from cosmogenic nuclides and geochemical mass balance, Geochim. Cosmochim. Acta 67 (2003) 4411–4427.
[18] C.S. Riebe, J.W. Kirchner, R.C. Finkel, Sharp decrease in long-term chemical weathering rates along an altitudinal transect, Earth Planet. Sci. Lett. 218 (2004) 421–434.
[19] D. Lal, Cosmic ray labeling of erosion surfaces: in situ nuclide production rates and erosion models, Earth Planet. Sci. Lett. 104 (1991) 424–439.
[20] E.T. Brown, R.F. Stallard, M.C. Larsen, G.M. Raisbeck, F. Yiou, Denudation rates determined from the accumulation of in situ-produced ^{10}Be in the Luquillo Experimental Forest, Puerto Rico, Earth Planet. Sci. Lett. 129 (1995) 193–202.
[21] D.E. Granger, J.W. Kirchner, R.C. Finkel, Spatially averaged long-term erosion rates measured from in situ-produced cosmogenic nuclides in alluvial sediment, J. Geol. 104 (1996) 249–257.
[22] C.S. Riebe, J.W. Kirchner, D.E. Granger, R.C. Finkel, Erosional equilibrium and disequilibrium in the Sierra Nevada, inferred from cosmogenic ^{26}Al and ^{10}Be in alluvial sediment, Geology 28 (2000) 803–806.
[23] C.S. Riebe, J.W. Kirchner, D.E. Granger, R.C. Finkel, Minimal climatic control on erosion rates in the Sierra Nevada, California, Geology 29 (2001) 447–450.
[24] P.V. Brady, S.A. Carroll, Direct effects of CO_2 and temperature on silicate weathering: possible implications for climate control, Geochim. Cosmochim. Acta 58 (1994) 1853–1856.
[25] J.W. Kirchner, R.C. Finkel, C.S. Riebe, D.E. Granger, J.L. Clayton, W.F. Megahan, Mountain erosion over 10-year, 10,000-year and 10,000,000-year time scales, Geology 29 (2001) 591–594.
[26] S.W. Trimble, The fallacy of stream equilibrium in contemporary denudation studies, Am. J. Sci. 277 (1977) 876–887.
[27] K.L. Moulton, R.A. Berner, Quantification of the effect of plants on weathering: studies in Iceland, Geology 26 (1998) 895–898.
[28] J.F. Banfield, W.W. Barker, S.A. Welch, A. Taunton, Biological impact on mineral dissolution: application of the lichen model to understanding mineral weathering in the rhizosphere, Proc. Natl. Acad. Sci. U. S. A. 96 (1999) 3404–3411.
[29] J.I. Drever, The effect of land plants on weathering rates of silicate minerals, Geochim. Cosmochim. Acta 58 (1994) 2325–2332.
[30] J.I. Drever, J. Zobrist, Chemical weathering of silicate rocks as a function of elevation in the southern Swiss Alps, Geochim. Cosmochim. Acta 56 (1992) 3209–3216.
[31] A.F. White, T.D. Bullen, D.V. Vivit, M.S. Schulz, D.W. Clow, The role of disseminated calcite in the chemical weathering of granitoid rocks, Geochim. Cosmochim. Acta 63 (1999) 1939–1953.
[32] A.E. Viau, K. Gajewski, P. Fines, D.E. Atkinson, M.C. Sawada, Widespread evidence of 1500 yr climate variability in North America during the past 14,000 yr, Geology 30 (2002) 455–458.
[33] L.G. Thompson, E. Mosley-Thompson, M.E. Davis, P.N. Lin, K. Henderson, T.A. Mashiotta, Tropical glacier and ice core evidence of climate change on annual to millennial time scales, Clim. Change 59 (2003) 137–155.
[34] V.C. LaMarche, Paleoclimatic inferences from long tree-ring records, Science 183 (1974) 1043–1048.